Ferromagnetism, paramagnetism, and thermally induced magnetism in photomagnetic Cr^{III}/Mn^{II} and Cr^{III} oxalates with the 7-methyl-3,3-diphenyl-3*H*-pyrano[3,2-*f*]quinolinium cation

S. M. Aldoshin,[a] N. A. Sanina,[a] R. B. Morgunov,[a] O. A. Fedorova,[b] S. V. Paramonov,[c,d] V. B. Lokshin,[d] F. B. Mushenok,[a] G. V. Shilov,[a] K. V. Bozhenko,[a] and D. V. Korchagin[a]*

[a]*Institute of Problems of Chemical Physics, Russian Academy of Sciences, 1 prosp. Akad. Semenova, 142432 Chernogolovka, Moscow Region, Russian Federation. Fax: +7 (496) 522 3507. E-mail: sanina@icp.ac.ru*
[b]*A. N. Nesmeyanov Institute of Organoelement Compounds, Russian Academy of Sciences, 28 ul. Vavilova, 119991 Moscow, Russian Federation. Fax: +7 (499) 135 5085*
[c]*D. I. Mendeleev Russian University of Chemical Technology, 9 pl. Miusskaya, 125047 Moscow, Russian Federation*
[d]*Interdisciplinary Center of Nanosciences in Marseille (CiNAM, CNRS UPR 3118), Campus de Luminy, Case 913, 13288 Marseille Cedex 9, France*

Single crystals of the new cationic chromene, 7-methyl-3,3-diphenyl-3*H*-pyrano[3,2-*f*]-quinolinium iodide ($C_{25}H_{20}NO)I$ (**1**), were synthesized. The crystal structure of the new compound was studied, and quantum chemical calculation for the open and closed forms were carried out. The bifunctional compounds containing mono- and bimetallic 3d metal (tris)oxalates with the chromenium cation, $(C_{25}H_{20}NO)_3[Cr(C_2O_4)_3]\cdot 4H_2O$ (**2**) and $(C_{25}H_{20}NO)[CrMn(C_2O_4)_3]\cdot H_2O$ (**3**), were prepared. Compound **1** is paramagnetic due to low-lying thermally excited states of the chromene molecules. At low temperatures (~2 K), the paramagnetic states are frozen, and the compound becomes diamagnetic. Compound **2** is paramagnetic and its magnetic properties are determined mainly by the Cr^{3+} ions and the thermally induced paramagnetic states of the chromene molecules. At high temperatures, the magnetic moment of compound **3** consists of the contributions of the paramagnetic Cr^{3+} and Mn^{2+} ions and the thermally induced paramagnetic states of chromenes. At low temperatures (2—3 K), the thermally induced magnetism of organic molecules is frozen, and the magnetically ordered (and, probably, spin-glass) state is observed in the two-dimensional network of metal oxalates (T_c = 3 K in the zero magnetic field). The UV irradiation leads to an increase in the magnetic moment of the compound in the paramagnetic region due to the generation of radiation defects.

Key words: molecular magnets, (tris)oxalates, polyfunctional compounds, photochromic compounds; chromenes, ferromagnetic substances, thermally induced paramagnetism.

The systematic studies of the synthesis, the structural and photochemical mechanisms of the transformations of different classes of photochromic compounds have been intensively carried out in the last 25 years.[1—4] Photochromic spiro systems (spiropyrans (SpP), spirooxazines (SpO), and chromenes) are still promising photochromic compounds for the design of information recording, storage, and processing systems and as optical switches for the properties of functional materials.[1] However, the photochromic transformations in the crystals of neutral SpP and SpO, which are accompanied by the C_{SpP}—O bond cleavage followed by the isomerization of the molecules, are extremely hindered because of the close packing of the molecules in the crystal lattices. Recently,[5—9] the salt forms of spiropyrans $[SpP]^+X^-$, which exhibit photochromic properties independent of the nature of the X^- anion in the crystals, have been synthesized and investigated. It was found that in the crystals of neutral SpP of the indoline series, the pyridopyran moieties of the molecules responsible for the photochromic transformations are closely packed to form stacks (Fig. 1, *a*), which hinders the photochromic transformations in the solid state.

On the contrary, in the crystals of the salts $[SpP]^+X^-$ containing the quaternary positively charged N^+ atom of the pyridopyran moiety (Fig. 1, *b*), the electrostatic interactions between the X^- anion ($X^- = I^-$) and the quater-

Published in Russian in *Izvestiya Akademii Nauk. Seriya Khimicheskaya,* No. 3, pp. 487—499, March, 2010.

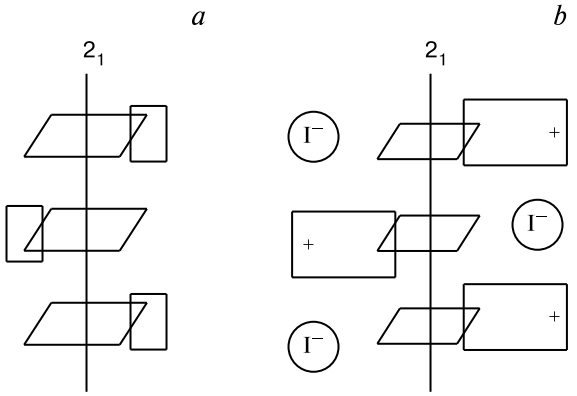

Fig. 1. Crystal structures of neutral SpP of the indoline series (*a*) and the salts $[SpP]^+I^-$ (*b*).

nized N^+ atom prevent[7—9] the formation of stacks of the pyridopyran moieties. In SpP salts, the indoline moieties form stacks, whereas the pyridopyran fragments together with the X^- anions are loosely packed between the stacks, thus providing the possibility of reversible photochromic transformations in the crystals. The packing of the salts $[SpP]^+X^-$ is independent of the size of the X^- anion, which was successfully replaced by paramagnetic[10] and ferromagnetic[11—14] anions, but the packing is very sensitive to the substituents in the indoline moiety of $[SpP]^+$.[9]

Hence, the detailed investigation of the crystal structures of salts of new spiro compounds can be of decisive significance for the prediction of photochromic transformations of the cations in the solid state. This is of importance for the search for promising salts of spiro systems as photochromic cation sublattices of hybrid crystals containing the magnetic anion sublattice, for the photocontrol of the intra- and intermolecular magnetic coupling, and the investigation of the effect of the photochromic sublattice on the bulk behavior of molecular magnets.[15] In the cations of salts of photochromic chromenes, as opposed to the $[SpP]^+X^-$ and $[SpO]^+X^-$ salts, there are no orbital n—σ* interactions resulting in the weakening of the C_{SpP}—O bond and favorable for photochromic transformations. These salts have another (vibration) mechanism of the C_{SpP}—O bond cleavage and are thermally more stable.[16] Hence, they would be promising photochromic structural blocks for the design of polyfunctional molecules. Besides, no data were available on the structures of the salt forms of chromenes.

In the present study, the structure of the new cationic chromene, *viz.*, 7-methyl-3,3-diphenyl-3*H*-pyrano[3,2-*f*]-quinolinium iodide (**1**), was investigated and quantum chemical calculations for the closed and open forms of this compound were carried out for the first time. The previously unavailable bifunctional compounds containing mono- and bimetallic 3d metal (tris)oxalates (**2** and **3**, respectively) with the chromenium cation were synthesized.

Experimental

The ^1H NMR spectra were recorded on a Bruker DRX-250 spectrometer (250 MHz).

Synthesis of 7-methyl-3,3-diphenyl-3*H*-pyrano[3,2-*f*]quinolinium iodide (1). 3,3-Diphenyl-3*H*-pyrano[3,2-*f*]quinoline (0.34 g, 1 mmol)[17] and iodomethane (3 mL) were heated in a sealed tube at 60 °C for 3 h. Then the reaction mixture was cooled, an excess of iodomethane was removed by evaporation, and the precipitate that formed was washed with diethyl ether. An amorphous bright-yellow powder was obtained in a yield of 0.46 g (96%). The analytical sample was isolated by the crystallization from ethanol, m.p. 210—213 °C. ^1H NMR ($CDCl_3$), δ: 4.82 (s, 1 H, Me); 6.53 (d, 1 H, H(2), J = 10.1 Hz); 7.25—7.46 (m, 11 H, H(1), 2 Ph); 7.82 (d, 1 H, H(5), J = 9.6 Hz); 8.08 (dd, 1 H, H(9), J = 8.8 Hz, J = 5.8 Hz); 8.17 (d, 1 H, H(6), J = 9.6 Hz); 9.17 (d, 1 H, H(10), J = 8.8 Hz); 10.10 (d, 1 H, H(8), J = 5.8 Hz). Found (%): C, 63.88; H, 4.35; N, 3.01. $C_{25}H_{20}INO$. Calculated (%): C, 62.90; H, 4.22; N, 2.93

Synthesis of 7-methyl-3,3-diphenyl-3*H*-pyrano[3,2-*f*]quinolinium tris(oxalato)chromate(III) trihydrate (2) and 7-methyl-3,3-diphenyl-3*H*-pyrano[3,2-*f*]quinolinium tris(oxalato)manganate(II)chromate(III) monohydrate (3). Molecular magnets **2** and **3** were synthesized according to the known method[13] in aerobic aqueous methanolic solutions at ~20 °C in the absence of UV irradiation. Compound **2.** The yield was 72%. Found (%): C, 68.43; H, 4.50; Cr, 3.83; N, 2.87; O, 28.31. $C_{81}H_{68}CrN_3O_{19}$. Calculated (%): C, 68.07; H, 4.76; Cr, 3.64; N, 2.94; O, 28.29. Compound **3.** The yield was 56%. Found (%): C, 50.03; H, 2.72; Cr, 7.00; Mn, 7.38; N, 1.93; O, 30.00. $C_{31}H_{22}CrMnNO_{14}$. Calculated (%): C, 50.34; H, 2.97; Cr, 7.04; Mn, 7.43; N, 1.89; O, 30.31.

Elemental analysis of polycrystalline samples of **2** and **3** was carried out in the Analytical Center of Collective Use of the Institute of Problems of Chemical Physics of the Russian Academy of Sciences by electron probe microanalysis and local X-ray spectral microanalysis with a Vega II XMU digital scanning electron microscope (Tescan, Brno, Czech Republic) equipped with a secondary electron (SE) detector, a backscatter electron (BSE) detector, and a low vacuum secondary tescan detector (LVSTD) fitted with YAG (yttrium aluminum garnet) crystals, using an INCA Energy 450 energy dispersive X-ray spectrometer equipped with a semiconducting Si(Li) detector (Oxford Instruments Ltd., Great Britain), and with an INCA Wave 700 wave length dispersive X-ray spectrometer (Oxford Instruments Ltd., Great Britain).

X-ray diffraction study was carried out on an automated four-circle Bruker P-4 diffractometer (graphite monochromator, λ(Mo-Kα) = 0.71073 Å, 293 K, θ/2θ-scanning technique). The X-ray diffraction data were collected from a poor-quality plate-like single crystal of **1** with dimensions 0.2×0.1×0.1 mm^3. The unit cell parameters were determined and refined based on 35 reflections in the θ angle range from 5 to 15°. The X-ray data set was collected in the θ angle range of 2.20—25.01°; the total number of independent reflections was 3476; the number of reflections with $I > 2\sigma(I)$ was 2570.

Principal crystallographic data are a = 7.845(2) Å, b = = 9.504(2) Å, c = 14.433(3) Å, α = 95.45(2)°, β = 102.38(2)°, γ = 100.07(2)°, V = 1025.0(4) $Å^3$, d_{calc} = 1.547 g cm^{-3}, space group P-1, Z = 2. The structure was solved by direct methods. The positional and thermal parameters of nonhydrogen atoms were refined first isotropically and then anisotropically by the full-matrix least-squares method. The hydrogen atoms in the

organic cation were positioned geometrically and refined using a riding model. The crystallographic data and the refinement statistics are given in Table 1. The interatomic distances and bond angles are listed in Tables 2. All calculations were carried out with the use of the SHELXTL program package.[18] The final R factors are $R_1 = 0.0395$ based on reflections with $I > 2\sigma(I)$ and $R_2 = 0.0646$ based on all reflections, GOOF = 1.010.

Magnetic properties of compounds 2 and 3. The magnetic moments (M) of powder samples were studied on a Quantum Design MPMS 5XL SQUID magnetometer. The temperature dependence of the magnetic moment was measured in the temperature range of 2—300 K at a constant magnetic field of the intensity $B = 0.1$ T. The dependence of the magnetic moment on the magnetic field strength was measured in the range $B = 0$—5 T at 2 K. In the course of measurements, the temperature was maintained within 0.01 K, and the magnetic field strength was maintained within 0.01 mT. Palladium was used as the standard, whose magnetic susceptibility is $560.1 \cdot 10^{-6}$ cm^3 mol^{-1} at $T = 293.1$ K and corresponds to the measured value with an accuracy of 99.5%.

Prior to the magnetic measurements, the samples were compacted between gelatin capsules, which were pressed into each other in a bottom-to-bottom fashion and hindered the motion and rotation of particles in the magnetic field. The absence of the effect of magnetic texturing on the experimental data was evidenced also by the fact that the residual magnetization was measured in a chaotic (unmagnetized) sample during cooling from room temperature in the zero field. Nevertheless, as will be shown below, the spontaneous magnetization was observed.

In addition, the data on the difference between FC (field cooling) and ZFC (zero field cooling) were obtained at the magnetic field strength of 0.005 T, in which the maximum magnetic energy of the particle with the magnetic moment of 8 μ_B is $8\mu_B gB = 5 \cdot 10^{-6}$ eV. In the magnetic field of the strength $B = 0.005$ T, the magnetic energy is 10^4 times lower than the average energy of thermal fluctuations kT per particle at $T = 300$ K (regardless of its mass). At 2 K, the magnetic energy of the particle in the magnetic field is 100 times lower than kT.

The samples were irradiated for 1 h with the use of a DRSh-1000 lamp outside the SQUID magnetometer with stirring of the powder in the course of irradiation. Then the powder was again pressed between gelatin capsules. The IR irradiation was protected with a water filter to prevent the heating of the sample. The temperature of the sample was monitored in the course of irradiation. The required wavelength range was isolated with the use of an UFS-1 light filter and focused onto the sample with the use of a quartz lens.

Table 1. Principal crystallographic data for compound **1**

Parameter	Characteristics
Molecular formula	$C_{25}H_{20}INO$
Molecular weight	477.32
Crystal system	Triclinic
Space group	P-1
Crystal dimensions/mm^3	0.2×0.1×0.1
a/Å	7.845(2)
b/Å	9.504(2)
c/Å	14.433(3)
α/deg	95.45(2)
β/deg	102.85(3)
γ/deg	100.07(2)
V/Å^3	1025.0(4)
Z	2
d_{calc}/g cm^{-3}	1.547
μ/mm^{-1}	1.577
F(000)	476
θ-Scan range/deg	2.20—25.01
Completeness at θ = 25.01 (%)	96.2
Number of measured reflections	4208
Number of independent reflections	3476
R_{int}	0.0257
Number of reflections with $I > 2\sigma(I)$	2570
Number of refined parameters	255
GOOF	1.010
R factors based on reflections with $I > 2\sigma(I)$	
R	0.0395
wR_2	0.0825
R factor (based on all reflections)	
R_1	0.0646
wR_2	0.0919

Results and Discussion

The detailed knowledge of the molecular and crystal structures of chromene salts, along with the previously studied[7—9] structures of the SpP salts, is of great importance for the prediction of the possibility of photochromic transformations of chromenium cations in the solid state. For this purpose, we investigated compound **1**, which is the starting cationic chromene in the synthesis of mono- and bimetallic complexes **2** and **3**, by X-ray diffraction.

The asymmetric unit of the crystal structure of **1** contains the organic cation and the iodide anion (Fig. 2). The organic chromenium cation consists of one pyran moiety and two phenyl fragments (see Fig. 2). The dihedral angle between the O—C(13)—C(2) and C(13)—C(14)—C(20)

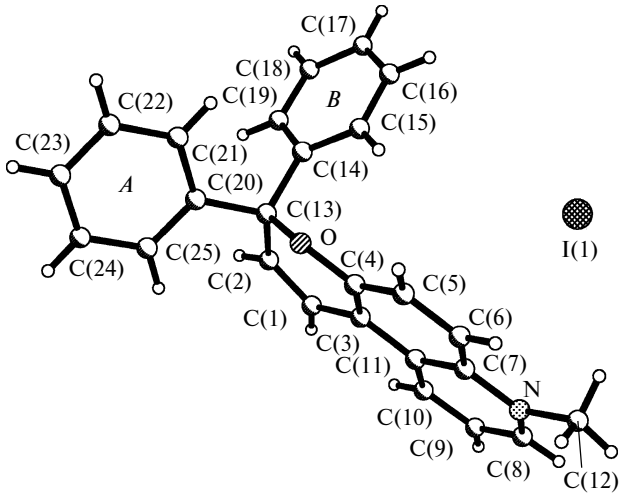

Fig. 2. Asymmetric unit of the crystal structure of compound **1**.

Table 2. Interatomic distances (*d*) and bond angles (ω) in the structure of salt **1**

Parameter	Value	Parameter	Value	Parameter	Value
Bond length	*d*/Å	Bond length	*d*/Å	Angle	ω/deg
O—C(4)	1.363(4)	C(10)—C(9)	1.369(6)	C(22)—C(4′)—C(3′)	119.7(5)
N—C(8)	1.323(5)	C(8)—C(9)	1.364(6)	C(4′)—C(22)—C(21)	120.3(5)
N—C(12)	1.472(5)	C(19)—C(18)	1.370(7)	C(17)—C(16)—C(15)	120.9(5)
C(13)—C(20)	1.518(5)	C(4′)—C(3′)	1.379(8)	C(2′)—C(3′)—C(4′)	119.9(5)
C(14)—C(15)	1.376(6)	C(18)—C(17)	1.355(7)	C(8)—N—C(7)	121.6(4)
C(3)—C(4)	1.375(5)	Angle	ω/deg	C(7)—N—C(12)	118.5(3)
C(3)—C(1)	1.451(5)			O—C(13)—C(20)	104.1(3)
C(20)—C(21)	1.383(6)	C(4)—O—C(13)	118.8(3)	O—C(13)—C(14)	109.0(3)
C(6)—C(5)	1.358(5)	C(8)—N—C(12)	119.9(3)	C(20)—C(13)—C(14)	113.0(3)
C(11)—C(10)	1.404(5)	O—C(13)—C(2)	110.1(3)	C(15)—C(14)—C(13)	122.9(4)
C(1)—C(2)	1.322(5)	C(2)—C(13)—C(20)	113.2(3)	C(4)—C(3)—C(11)	118.1(3)
C(2′)—C(3′)	1.376(7)	C(2)—C(13)—C(14)	107.4(3)	C(11)—C(3)—C(1)	124.2(3)
C(15)—C(16)	1.391(7)	C(15)—C(14)—C(19)	118.6(4)	O—C(4)—C(5)	115.6(3)
C(4′)—C(22)	1.365(8)	C(19)—C(14)—C(13)	118.4(4)	C(21)—C(20)—C(2′)	118.2(4)
C(21)—C(22)	1.392(7)	C(4)—C(3)—C(1)	117.7(3)	C(2′)—C(20)—C(13)	120.5(4)
C(16)—C(17)	1.359(7)	O—C(4)—C(3)	122.5(3)	C(10)—C(11)—C(7)	118.8(4)
O—C(13)	1.464(4)	C(3)—C(4)—C(5)	121.8(3)	C(7)—C(11)—C(3)	118.7(3)
N—C(7)	1.392(5)	C(21)—C(20)—C(13)	121.3(4)	C(9)—C(10)—C(11)	120.0(4)
C(13)—C(2)	1.510(5)	C(5)—C(6)—C(7)	120.2(4)	C(6)—C(7)—C(11)	120.8(3)
C(13)—C(14)	1.526(6)	C(10)—C(11)—C(3)	122.5(3)	C(3′)—C(2′)—C(20)	121.3(5)
C(14)—C(19)	1.396(6)	C(2)—C(1)—C(3)	119.7(3)	N—C(8)—C(9)	121.9(4)
C(3)—C(11)	1.438(5)	C(6)—C(7)—N	121.4(3)	C(6)—C(5)—C(4)	120.5(4)
C(4)—C(5)	1.404(5)	N—C(7)—C(11)	117.8(3)	C(18)—C(19)—C(14)	119.9(4)
C(20)—C(2′)	1.382(6)	C(1)—C(2)—C(13)	122.9(3)	C(20)—C(21)—C(22)	120.6(5)
C(6)—C(7)	1.385(5)	C(14)—C(15)—C(16)	119.8(4)	C(17)—C(18)—C(19)	121.4(5)
C(11)—C(7)	1.420(5)	C(8)—C(9)—C(10)	119.9(4)	C(18)—C(17)—C(16)	119.4(5)

planes is 86.3°. The dihedral angles between the O—C(13)—C(2) plane of the pyran moiety and the planes of the phenyl rings *A* and *B* are 100.6 and 115.8°, respectively. The dihedral angle between the planes of the phenyl rings *A* and *B* is 80.3°. The distances from the O atom of the pyran moiety to the C(15) atom of the phenyl ring *B* and the C(21) atom of the phenyl ring *A* are 2.761 and 3.157 Å, respectively. The shortest distances between the carbon atoms of the phenyl fragments *A* and *B* are as follows: C(14)...C(21), 2.923 Å; C(19)...C(24), 3.121 Å.

In Ref. 19, the molecular and crystal structures of spiro(1,3,3-trimethylindolino-2,3′-[3*H*]pyrano[3,2-*f*]-quinoline) and its derivative, *viz.*, spiro(1,3,3,7′-tetramethylindoline-2,3′-[3*H*]pyrano[3,2-*f*]quinolinium) iodide containing the quinoline fragment, were determined. As in indolinospiropyran, the pyranopyridine moiety in the chromenium cation is nonplanar. The bending angles along the O—C(2) and O—C(1) lines are $\alpha = 25.4°$ and $\beta = 5.8°$, whereas the corresponding angles in indolinospiropyran are 18.90 and 14.6°. The C(13)—O and O—C(4) bond lengths in compound **1** are 1.464(4) and 1.363(4) Å, respectively. and are equal within experimental error to the corresponding bond lengths in the spiropyran cation[19] (1.467(6) and 1.359(6) Å). The other bond lengths in the pyranopyridine moieties are also equal within experimental error (maximum threefold errors). The observed C(13)—O bond length is larger than the standard C—O bond lengths in six-membered oxygen-containing heterocycles (1.41—1.43(1) Å). The O—C(13)—C(2) and C(14)—C(13)—C(20) bond angles at the carbon atom C(13) are 110.1(3) and 113.0(3)°, respectively. In spiropyran, the corresponding angles at the spiro atom shared by two rings are 117.1(5) and 103.4°(4).

The C_{Sp}—O bond in spiropyrans is elongated due to orbital interactions between the nitrogen lone pair and the antibonding σ* orbital of the C_{Sp}—O bond, which leads to a weakening of this bond, resulting in that it can be efficiently cleaved in the photoexcited state. In the chromenium cation, the C—O bond appeared to be equal to that found in spiropyrans; however, efficient photochromic transformations analogous to those observed in spiropyran salts, were detected neither in the solid state nor in solution. A comparison of the X-ray diffraction patterns of crystalline powders of **1** before and after irradiation revealed no differences, which is indicative of the absence of photochromic transformations in the crystals.

The crystal structure of salt **1** is presented in Figs 3 and 4.

The organic cations (see Fig. 3) form a block packing with channels occupied by I^- anions. The I^- anions are at distances of 4.12 and 4.50 Å from the positively charged

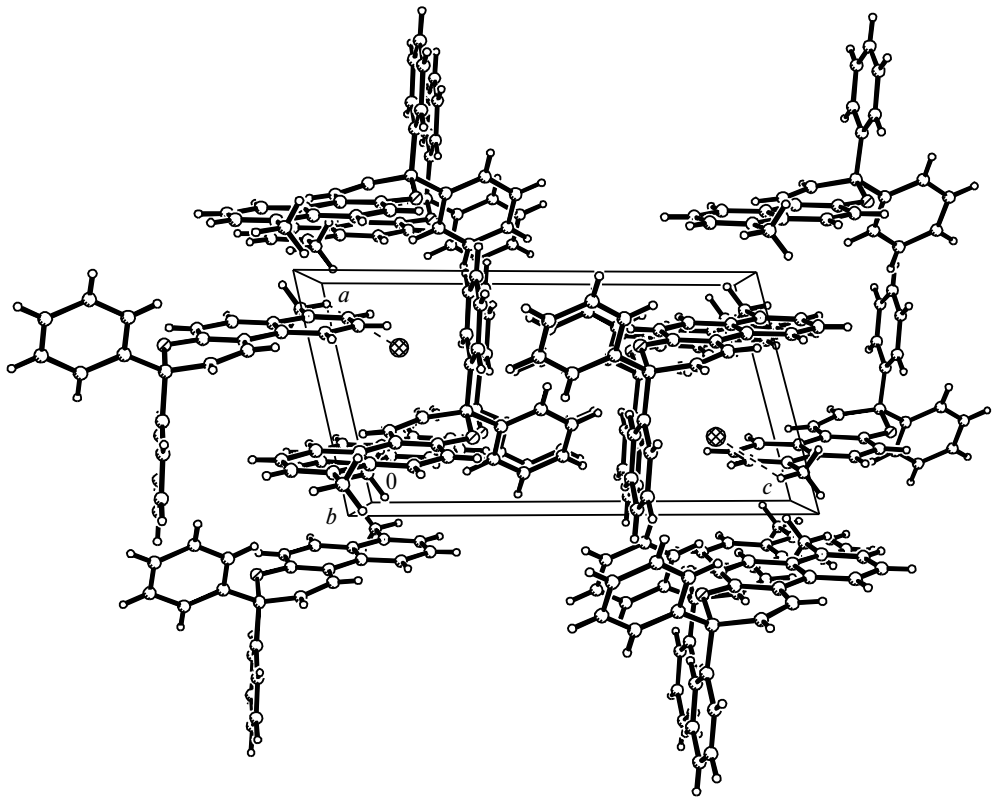

Fig. 3. Crystal structure of salt **1** projected onto the *ac* plane of the crystal lattice.

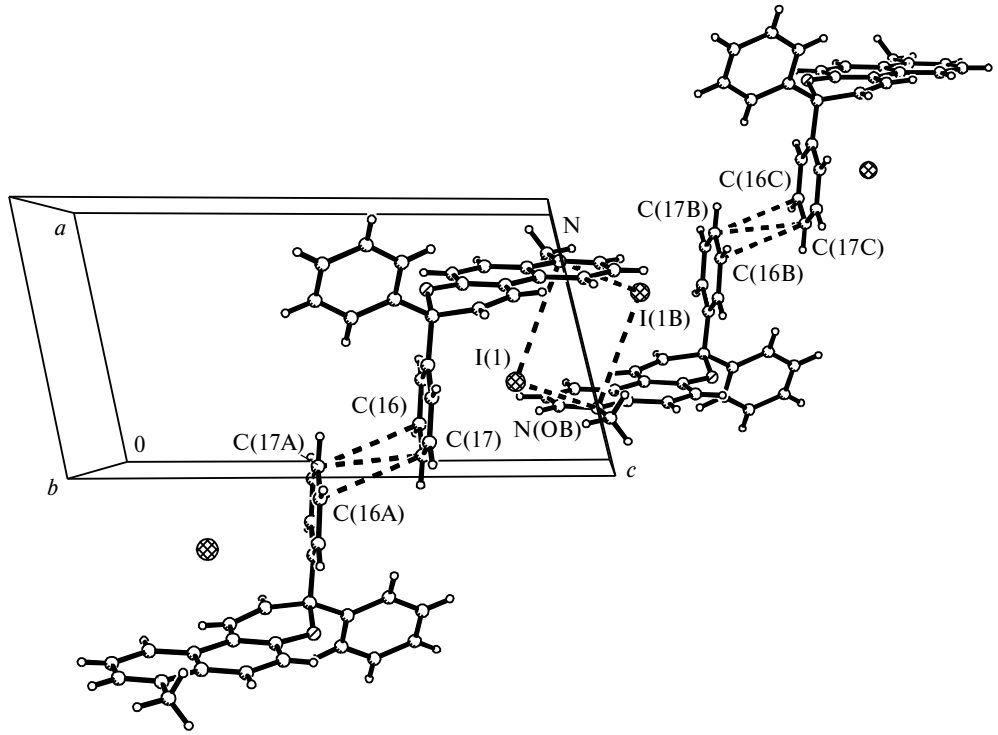

Fig. 4. Fragment of the crystal structure of salt **1** (the fragments involved in van der Waals interactions are connected by dashed lines).

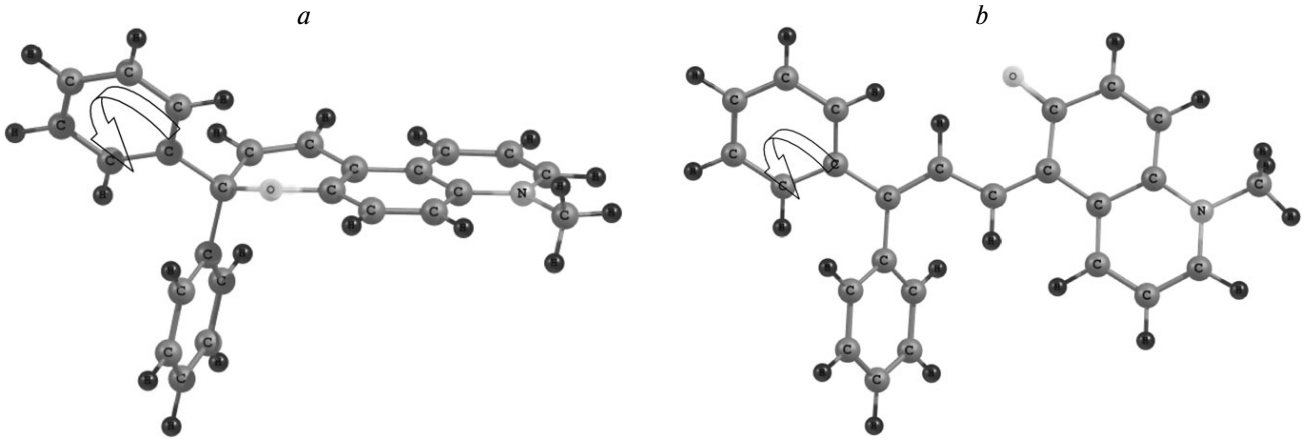

Fig. 5. Structures of the closed (*a*) and open (*b*) forms of compound **1**; E_{tot}(B3LYP/6-31G) = −1094.1949497 and −1094.1898504 au, respectively; the torsion angle (*D*) is indicated by an arrow.

nitrogen atoms of the cations related by the inversion center (1/2 0 1/2) and the translation (0 −1 1). The fragment of the crystal structure is shown in Fig. 4, where the nearest I^- and N^+ ions are connected by dashed lines. The shortest distance between the I^- anion and the C(10) atom is 3.88 Å, which is longer than the corresponding distance (3.76 Å) in the structure reported in the study.[19] In the crystal structure, there are short intermolecular contacts between the carbon atoms (C(16)...C(17), 3.396 Å; C(17)...C(17), 3.152 Å) of the phenyl fragments *B* of two adjacent cations related by the inversion center (0 0 1/2) (see Fig. 4). The van der Waals energy of these interactions is −3.3 kcal.

The contribution of the van der Waals interactions to the total crystal lattice energy is −29.80 kcal.

In spiropyran salts exhibiting photochromic properties, the cations are generally arranged so that the indoline fragments form 2_1 stacks, whereas the pyran moieties deviate from the stacks in different directions. In this crystal packing, the distance between the pyran fragments is equal to the full period of the crystal lattice; in particular, the period reported in the study[19] is 11.338 Å. In the crystal structure of compound **1**, such stacks are absent. The translationally related chromenium cations form columns along the *b* axis of the unit cell. The distance between the cations in the columns is 9.504(2) Å. This could provide favorable conditions for photochemical transformations. However, the phenyl fragment in each cation, in particular, the ring *B*, forms short contacts with the analogous ring of the cation from the adjacent column (see Fig. 4), which obviously limits the possibility of moving this part of the cation in the case of its rearrangement. The pyran moiety of each cation is involved in Coulombic interactions with two I^- anions (see Fig. 4). Each of these anions is, in turn, involved in electrostatic interactions with the pyran moiety of the cation from the adjacent column. As a result, the crystal structure consists of associates. Assuming that the absence of photochromic transformations is associated only with the crystal structure of this compound, the fact that chromene cannot exist in the open form in the solid state can be attributed to the revealed features of the crystal structure.

We compared the isomerization of the closed forms of chromene salt **1** and the iodide salt of spiropyran of the quinoline series[19] to the open forms in the ground state by quantum chemical methods.

The full geometry optimization of the open and closed forms of the compounds under consideration (Figs 5 and 6) was carried out at the B3LYP/6-31G level of theory with the use of the GAUSSIAN-03 program.[20] According to the quantum chemical calculations (Tables 3 and 4), the closed form of **1** is thermodynamically more stable. The total energy of the closed form is ~3.2 kcal mol^{-1} lower than that of the open form. For the spiropyran of the quinoline series,[19] the situation is opposite. Thus, the open

Table 3. Total ($-E_{tot}$) and relative energies (E_{rel}) of the structure of compound **1** at different torsion angles *D*

D/deg	$-E_{tot}$/hartree	E_{rel}	
		hartree	kcal mol^{-1}
−180	1094.189844	0.005106	3.203878
−120	1094.171849	0.0231	14.49567
−90	1094.157571	0.037379	23.45545
−60	1094.169547	0.025402	15.9402
0	1094.19495	0	0
30	1094.187097	0.007852	4.927522
60	1094.143023	0.051927	32.58465
90	1094.094887	0.100063	62.79034
105	1094.162886	0.032064	20.12042
120	1094.172396	0.022554	14.15286
150	1094.185666	0.009283	5.825426
180	1094.189844	0.005106	3.203878

Table 4. Total ($-E_{tot}$) and relative energies (E_{rel}) of the structure of the spiropyran salt at different torsion angles D

D/deg	$-E_{tot}$/hartree	E_{rel}	
		hartree	kcal mol^{-1}
−180	1074.550218	0	0
−150	1074.541479	0.008739	5.483935
−120	1074.531179	0.019039	11.94704
−105	1074.520742	0.029477	18.4968
−90	1074.514941	0.035278	22.13705
−60	1074.532131	0.018088	11.35009
−30	1074.536707	0.013511	8.47835
0	1074.543629	0.006589	4.134914
30	1074.537586	0.012633	7.927146
60	1074.489459	0.06076	38.12732
90	1074.506769	0.043449	27.265
105	1074.517919	0.032299	20.26826
120	1074.527779	0.02244	14.08107
150	1074.541075	0.009143	5.737387

form is thermodynamically more stable; the total energy of this form is ~4.1 kcal mol^{-1} lower than that of the closed form.

The isomerization of the chromene and spiropyran salts was analyzed taking into account the energy barriers in the corresponding potential energy curves (Fig. 7). The potential energy curves for the isomerization in the singlet ground state were calculated with a gradual increase in the C—C—C—C torsion angle with a step of 30° (D, see Figs 5 and 6) using the optimization of all other geometric parameters for each fixed value of D. The energy E_{rel} is the difference between the total energy of the system at a particular value of D and the minimum total energy of the system. For **1**, this is the energy of the closed form. On the contrary, this is the energy of the open form for the spiropyran salt.

The calculated energy barriers for the isomerization of compound **1** (23.5 kcal mol^{-1}) and the spiropyran salt (22.1 kcal mol^{-1}) indicate that these processes are almost equally probable (see Fig. 5).

In addition, the quantum chemical calculations at the same B3LYP/6-31G level of theory (Table 5) showed that the singlet-triplet splitting for these molecules (for both the closed and open forms) is ~1.5 eV.

(Tris)oxalates **2** and **3** with the 7-methyl-3,3-diphenyl-3*H*-pyrano[3,2-*f*]quinolinium cation were synthesized in aerobic aqueous methanolic solutions at room temperature according to Scheme 1.

Due to the higher stability of the closed form of chromene salt **1** (Fig. 8, *a*) compared to the open form (according to the above quantum chemical calculations), the reaction can be performed in polar solvents in the absence of UV irradiation, as opposed to the previously synthesized systems[13,14] containing the cations of spiro-

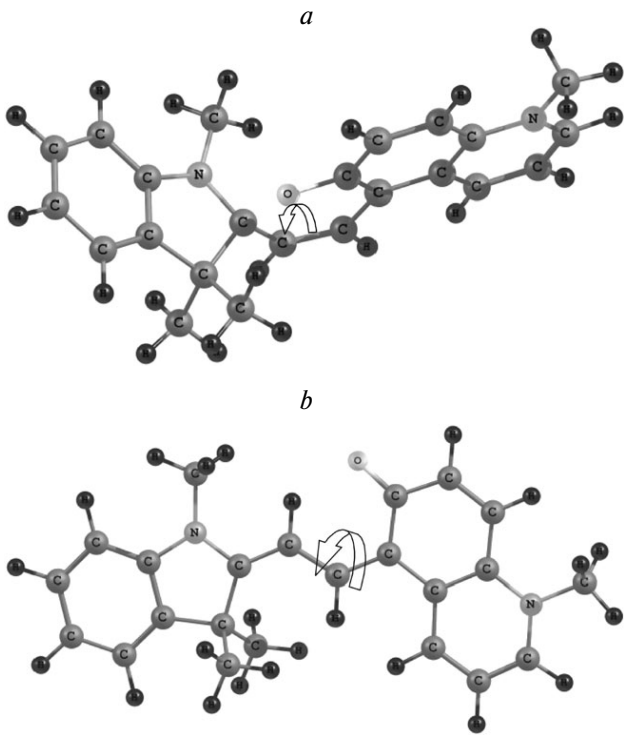

Fig. 6. Structures of the closed (*a*) and open (*b*) forms of spiropyran; E_{tot}(B3LYP/6-31G) = −1074.5436288 and −1074.5502182 au, respectively; the torsion angle (D) is indicated by an arrow.

Scheme 1

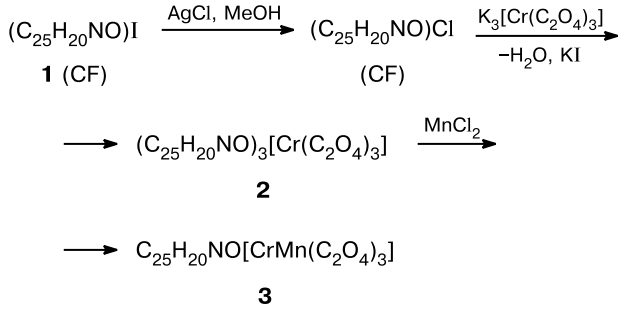

CF is the closed form

Table 5. Calculated total energies and singlet-triplet splittings of spiropyran (SpP) and chromene (Hr) salts in the singlet (S) and triplet (T) states

Compound (form)	$-E_{tot}$/au		Δ_{ST}*/eV
	S	T	
SpP (closed)	1074.8186978	1074.7625399	1.53
SpP (open)	1074.8221086	1074.7717584	1.37
Hr (closed)	1094.1949496	1094.1339451	1.66
Hr (open)	1094.1898504	1094.1420973	1.30

* Δ_{ST} is the singlet-triplet energy difference.

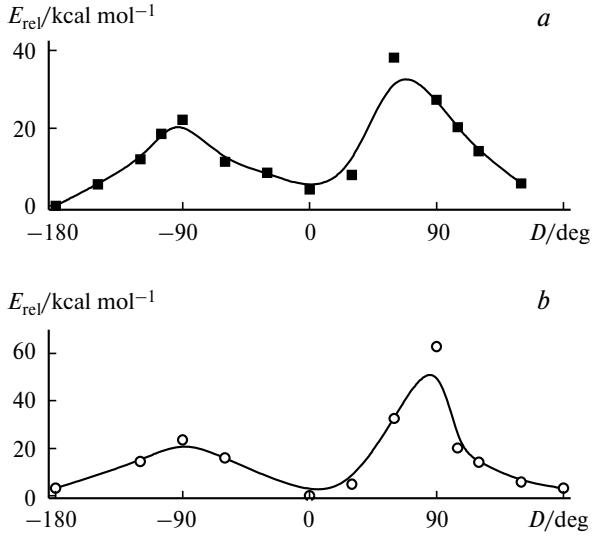

Fig. 7. Potential curves of the isomerization of the chromene (*a*) and spiropyran salts (*b*).

pyrans of the indoline series with the quaternary pyridine nitrogen atom N^+ introduced into the side aliphatic chain. Products **2** and **3** were isolated in high yield. Polycrystals of **2** (Fig. 8, *b*) are yellow-green in color and are readily soluble in polar solvents. Polycrystals of **3** (Fig. 8, *c*), like the previously synthesized bimetallic (tris)oxalate and dithiooxalate complexes with tetraalkylammonium[21—23] and spiropyran[11—14] cations, are emerald-green in color and are insoluble in water and other solvents.

In the present study, we investigated the magnetic properties of new compounds **1**—**3**. At 2 K, compound **1** is diamagnetic. However, an increase in the temperature leads to the transformation of **1** into the paramagnetic state. The effective magnetic moment increases from zero at 2 K to 3.5 μ_B at 250 K (Fig. 9). The temperature dependence substantially deviates from the Curie law, according to which μ_{eff} = const at $T > 10$ K. Previously,[24] we have observed the similar dependence for ions of spiropyran molecules. This dependence is attributed to a decrease in the number of paramagnetic particles as the sample is cooled and is well known as a fingertip of the triplet paramagnetism of the low-lying states of organic molecules, which are thermally occupied as the temperature increases.[25] In our recent study,[24] we have reported the thermally induced paramagnetism of spiropyran ions. It would be expected that chromene molecules can also exhibit thermally induced paramagnetism. This phenomenon is well known for many organic compounds.[24—33] From Fig. 9 it follows that the thermally induced paramagnetism is observed also for chromenium ions, if other paramagnetic species are absent in the compounds. An attempt to approximate the experimental dependence by the classical formula

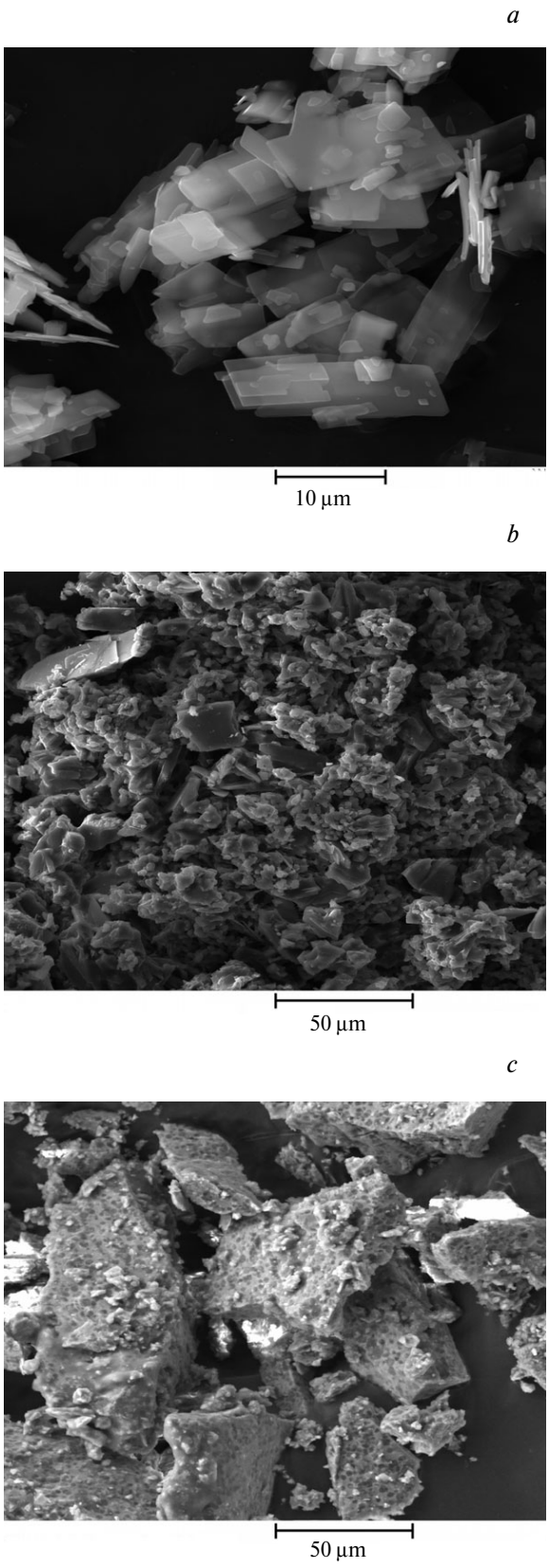

Fig. 8. Photographs of polycrystals of compounds **1** (*a*), **2** (*b*), and **3** (*c*).

for the triplet paramagnetism corrected for the paramagnetic impurity

$$\mu = 4g\mu_B\sqrt{\frac{N_A/k}{3+\exp[E^T/(kT)]}+c} \quad (1)$$

(g is the g factor, N_A is Avogadro's number, k is the Boltzmann constant, and E^T is the energy difference between the triplet ($S=1$) and singlet ($S=0$) states of the chromene molecule) showed that the theory is in qualitative agreement with the experimental data (see Fig. 9, curve *1*).

However, we failed to obtain the exact approximation. Presumably, this is associated with a substantial difference in the activation energies E^T. Taking into account the Gaussian energy distribution of the molecules, the equation can be written as follows:[26]

$$\mu_{eff}(T) = \frac{4\mu_B g}{(T-T_0)^{1/8}}\sqrt{(\pi^2 E^T/k^{5/4})^{1/4}N_A}\cdot \cdot\exp\left\{-\sqrt{E^T/[k(T-T_0)]}\right\}+c, \quad (2)$$

where $g = 2$ and $T_0 = 13$ K is the constant that takes into account the exchange and dipole-dipole interactions between the spins of chromenes. The approximation by the latter formula more accurately describes the experimental dependence, except for the low-temperature region (2—10 K), where the magnetic moment of the sample dramatically decreases and the accuracy of measurements is very low. The activation energy calculated using the approximation by Eq. (2) ($E^T = 0.016$ eV) is typical of low-lying excited states of organic molecules.[25—33] Thus, ionized chromene molecules exhibit thermally induced paramagnetic states.

The investigation of the magnetic properties of polycrystals of **2** showed that hybrid compound **2** is paramagnetic. The temperature dependence of the effective magnetic moment μ_{eff} and the dependence of the molar magnetic moment M on the external magnetic field B (at $T = 2$ K) are shown in Figs 10 and 11, respectively. At 2—5 K, the effective magnetic moment is 3.89 μ_B and is close to the theoretical value $\mu_{eff} = g[S(S+1)]^{1/2} = 3.87\ \mu_B$ calculated for the non-interacting spins of Cr^{3+} ions. The fact that at 2 K, only Cr^{3+} ions make the contribution to the magnetic moment is also evidenced by the approximation of the magnetic field dependence of the magnetic moment by the Brillouin function (see Fig. 11), from which the average spin was estimated as 3/2, *i.e.*, this spin is equal to the spin of Cr^{3+} ion. An increase in the temperature up to 300 K is accompanied by a gradual increase in the effective magnetic moment (see Fig. 10), which is similar to the dependence of μ_{eff} for compound **1** (*cf.* Fig. 9). It is reasonable to explain the increase in μ_{eff} with increasing temperature by the contribution of the thermally induced magnetism of the sublattice of the chromene molecules. It should be noted that the increase in the magnetic moment of the sample compared to the value determined for the paramagnetic states of Mn^{2+} and Cr^{3+} ions is larger than that expected for the triplet states. This can be associated with the fact that the spin of the thermally excited molecules exceeds S = 1. At low temperatures, the Cr^{3+} sublattice makes the major contribution to the magnetization. Hence, it is impossible to determine the spin of chromene molecules by the analysis of the Brillouin function. Another explanation is that the number of chromene molecules per formula unit is larger than the calculated value (for example, if these molecules are present as an impurity).

Complex **2** was used as the starting building block for the preparation of bimetallic compound **3** with the $[CrMn(C_2O_4)_3]^-$ anion. The temperature dependence of the effective magnetic moment of compound **3** shows

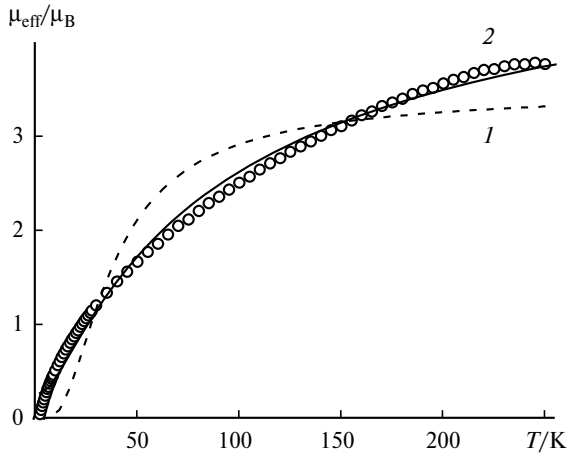

Fig. 9. Temperature dependence of the effective magnetic moment (μ_{eff}) of compound **1** in a constant magnetic field of the intensity $B = 5$ mT. The lines *1* and *2* represent the approximations by Eqs (1) and (2), respectively (see the text).

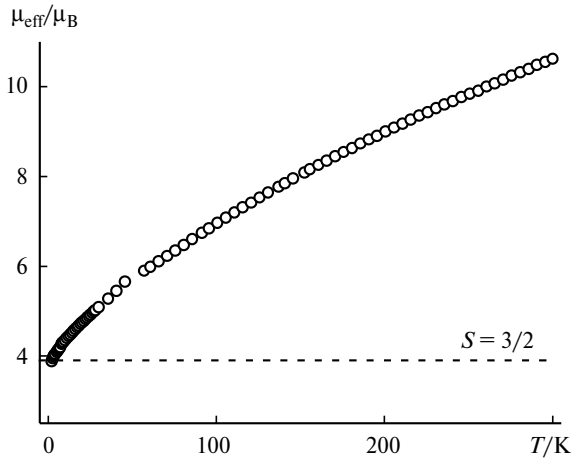

Fig. 10. Temperature dependence of the effective magnetic moment (μ_{eff}) of compound **2** in a constant magnetic field of the intensity $B = 1$ T. The calculated effective magnetic moment of Cr^{3+} ions ($S = 3/2$) is indicated by a dashed line.

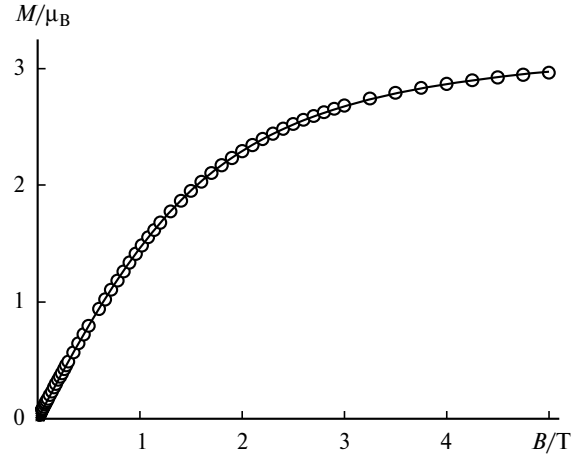

Fig. 11. Magnetic moment (M) of compound **2** *versus* the external magnetic field B at $T = 2$ K. The solid line represents the approximation by the Brillouin function with the spin $S = 3/2$.

a sharp decrease in μ_{eff} in the low-temperature region (2—10 K) and a gradual increase in μ_{eff} at temperatures up to 300 K (Fig. 12). The high values of μ_{eff} at low temperatures indicate ferromagnetic interactions, which occur in a two-dimensional network of metal oxalates between Cr^{3+} and Mn^{2+} ions. To answer the question whether these interactions lead to the ferromagnetic spin ordering in the anion sublattice, we obtained the temperature dependences of the effective magnetic moment of the sample in a weak magnetic field (5 mT) under two different operating conditions: after cooling in the zero field and after cooling in a field of 5 T (see the inset in Fig. 12). These dependences were found to be identical at high temperatures (10—300 K) and differ at low temperatures (2—10 K). This difference proves the magnetic spin ordering, which can be either ferromagnetic (parallel spins of Cr^{3+} ($S = 3/2$) and Mn^{2+} ($S = 5/2$) ions) or ferrimagnetic (antiparallel spins of these ions). The measurements of the temperature dependence of the spontaneous magnetization of the sample in the absence of a constant magnetic field (Fig. 13) confirmed the magnetic ordering in the system. The sample was cooled in the zero magnetic field from 300 to 2 K. Prior to the measurements, the magnetic field was not applied to the sample. The magnetic moment cannot be observed in paramagnetic samples with weak ferromagnetic correlations at low temperatures in the zero magnetic field and it directly proves the existence of the magnetically ordered state. In addition, this dependence allows the precise determination of the Curie temperature $T_c = 3$ K, which is shifted to higher temperatures in non-zero fields, being the increasing function of the magnetic field. In a magnetic field of 5 T, $T_c = 15$ K. The strong dependence of T_c on the magnetic field is characteristic of the two-dimensional ferromagnetism. This is in good agreement with the crystal structure of the compound under study, in which the oxalate complexes form two-dimensional networks. However, the sensitivity of T_c to the magnetic field strength can be attributed also to the fact that there is an impurity of the spin-glass state with chaotic frozen orientations of the spins.

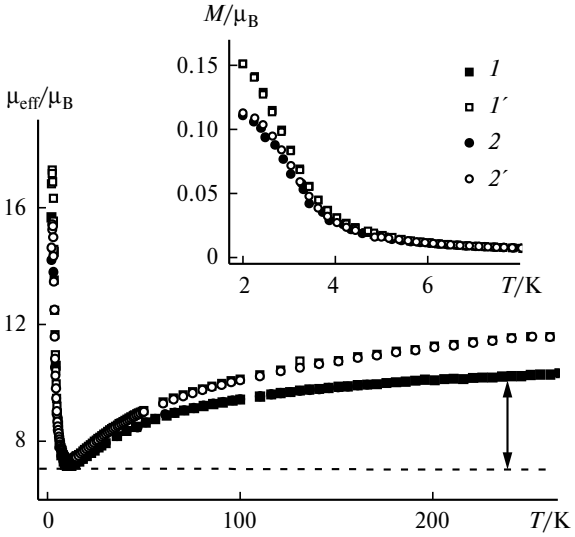

Fig. 12. Temperature dependence of the effective magnetic moment (μ_{eff}) for sample **3** cooled in a field of the intensity $B = 1$ T (*1*) and in the zero field (*2*), *1′* and *2′* are the corresponding dependences after white light irradiation. The calculated effective magnetic moment for a system of paramagnetic Cr^{3+} ($S = 3/2$) and Mn^{2+} ($S = 5/2$) ions is indicated by the horizontal dashed line; the arrow corresponds to the contribution of the chromenium cations. The low-temperature fragments of the plots of the magnetic moment M *versus* the temperature before (*1*, *2*) and after (*1′*, *2′*) irradiation are shown in the insets.

It should be noted that the moments μ_{eff} for the data presented in Fig. 12 were calculated according to the formula for a paramagnetic sample: $\mu_{eff} = [8MT/(\nu B)]^{1/2}$, where M is the magnetic moment of the sample, ν is the amount of the compound, and B is the magnetic field

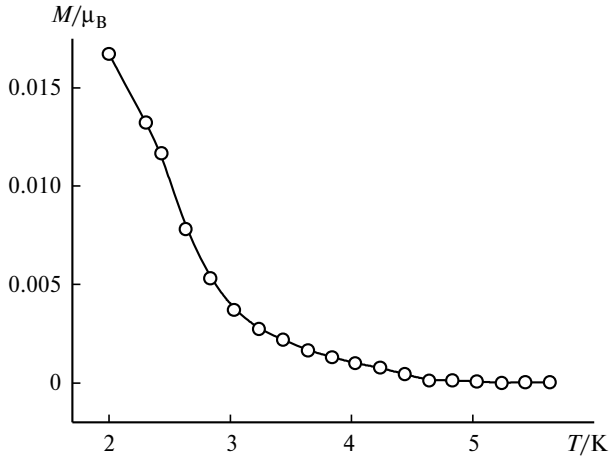

Fig. 13. Temperature dependence of the spontaneous molar magnetization of sample **3** in the zero field.

induction. In the case of ferromagnetic interactions, this equation cannot be used, *i.e.*, the vertical axis in Fig. 12 characterizes only the high-temperature part of the dependence. Hence, the inset (see Fig. 12) gives M in Bohr magnetons per unit cell (as is commonly used for ferromagnets). The low values of M are attributed to the fact that the magnet is far from saturation in a magnetic field of 5 mT (see below).

In attempting to obtain the hysteresis loop for M, we observed a very weak coercive force (1.5 mT) comparable with the residual magnetization field (1.1 mT) of the SQUID magnetometer (Fig. 14). It should be noted that, as opposed to the study,[11] we did not observe an increase in the coercive force and the saturation field after the exposure of the crystal under white or UV light. However, the magnetic field dependence substantially deviates from the Brillouin function (*cf.* Fig. 11). There are a sharp increase in weak fields and a gradual approach to the saturation. This may indicate that the powder contains magnetized particles with the orientation of the easy magnetization axis along the field direction, as well as particles in which the easy magnetization axis is perpendicular to the field direction. The saturation of the effective magnetic moment was not achieved in the available magnetic field range. In Fig. 14, the calculated moments μ_{eff} for the ferromagnetic saturation (2 μ_B) and the antiferromagnetic saturation (8 μ_B) are indicated by horizontal lines. It can be seen that M in compound **3** is larger than 2 μ_B and tends to 8 μ_B in high magnetic fields. This allows the identification of the magnetically ordered state as the ferromagnetism.

The magnetic field dependence can be interpreted in another way. For example, it can be suggested that the ferrimagnetic ordering occurs in the phase of compound **3**, which leads to the rapid saturation already in weak fields. A further increase in the magnetic field strength can lead to the so-called "para-process" resulting in the noncollinear orientation of the spins. In our opinion, it is difficult to experimentally confirm (or deny) this hypothesis for powder samples based on the results of magnetic measurements. Besides, the high-field part of the plot $M(B)$ is essentially nonlinear (except for the region consisting of the last four points), and its contribution is significantly higher than the expected ferrimagnetic moment. Hence, the hypothesis about the ferrimagnetic state seems to be less probable, although it cannot be completely ruled out based on the results of our measurements.

The ferromagnetism is often observed in impurity clusters and metallic inclusions and it makes a substantial contribution to the magnetization of the samples. The cluster magnetism is characterized by the strong frequency dependence of the magnetic susceptibility measured in an alternating magnetic field. To elucidate the role of magnetic clusters, we obtained the temperature dependences of the real (χ') and imaginary (χ'') parts of the magnetic susceptibility at frequencies of 1400 and 100 Hz (Fig. 15).

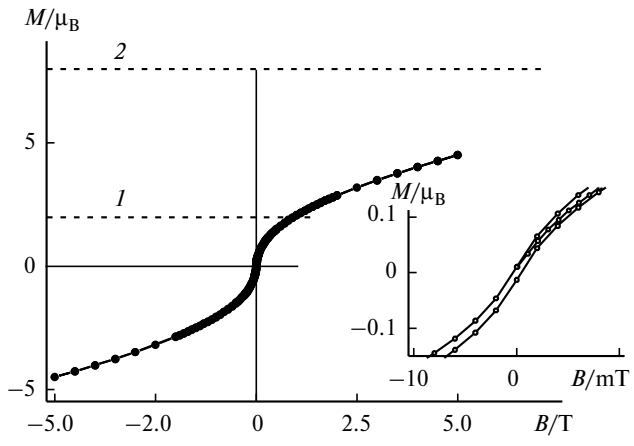

Fig. 14. Plot of the magnetic moment (M) *versus* the external magnetic field strength B at T = 2 K. The calculated effective magnetic moments of a ferrimagnet (*1*) and a ferromagnet (*2*). The low-field part of the plot $M(B)$ is shown in the inset.

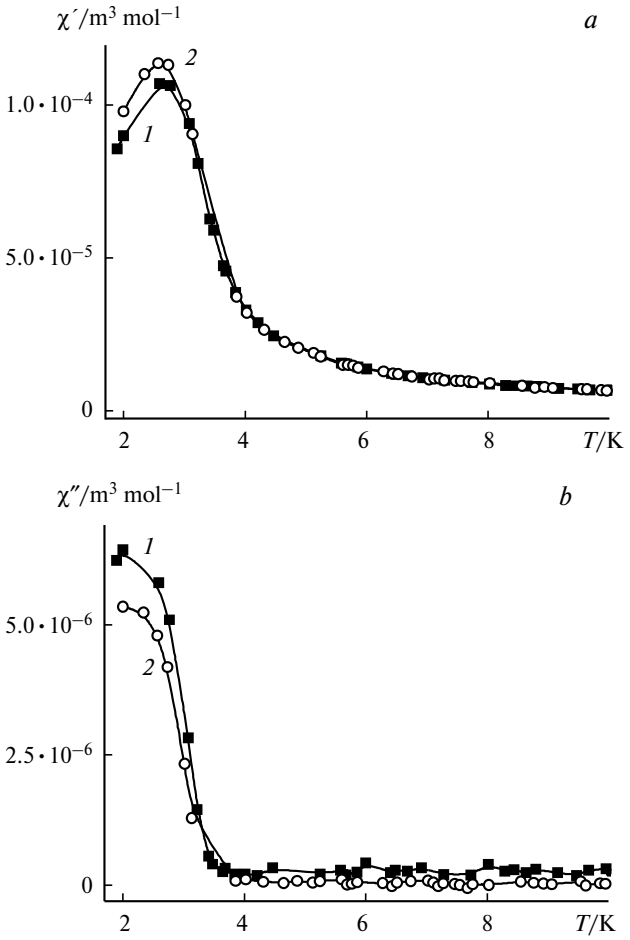

Fig. 15. Temperature dependences of the real χ' (*a*) and imaginary χ'' (*b*) parts of the dynamic (AC) magnetic susceptibility measured in an alternating magnetic field of the intensity B = 0.3 mT at frequencies of 1400 (*1*) and 100 Hz (*2*).

The positions of the maxima in these curves almost coincide. This is characteristic of both spin-glass and ferromagnetic states, which cannot be distinguished based on the available experimental data. In our experiments, the existence of frustrated spin states and the appearance of the spin-glass phase are also possible against the background of the magnetically ordered phase.

At first glance, the conclusions about the ferromagnetic state of compound **3** at low temperatures are in contradiction with the high-temperature data (see Fig. 13). Generally, a minimum in the $\mu_{eff}(T)$ curve, which is characteristic of the ferrimagnetic state, is not observed for ferromagnets at $T > T_c$. However, the data on the magnetic moments at high temperatures cannot be accounted for only by the ferrimagnetism because, in this case, μ_{eff} should tend to 7.07 μ_B at 300 K; the latter value is the theoretically calculated moment for a system consisting of two noninteracting spins of Cr^{3+} ($S = 3/2$) and Mn^{2+} ($S = 5/2$) (see Fig. 14, the horizontal dashed line). In our experiments, μ_{eff} in the paramagnetic phase tends to 10 μ_B at 300 K. Therefore, the excessive value of μ_{eff}, which differs by 3 μ_B from the calculated value at $T = 300$ K, is not a consequence of ferro- or ferrimagnetic correlations. This value can be attributed to the contribution of one more magnetic subsystem consisting of organic chromene molecules (see Fig. 10).

It seems not accidental that μ_{eff} at the minimum of the $\mu_{eff}(T)$ curve at 5 K is equal to the calculated value $\mu_{eff} = g[S_{Cr}(S_{Cr} + 1) + S_{Mn}(S_{Mn} + 1)]^{1/2} = 7.07\ \mu_B$ (see Fig. 12). At 10 K, the triplet paramagnetism of chromenes is almost "frozen," whereas the ferromagnetic ordering does not appear ($T > T_c$). Hence, only weakly interacting Cr^{3+} and Mn^{2+} ions contribute to μ_{eff}. This accounts for the value $\mu_{eff} = 7.07\ \mu_B$ at the minimum of the $\mu_{eff}(T)$ curve, as well as for the presence of the minimum.

After the UV irradiation for 2 h using a light filter, the $\mu_{eff}(T)$ curves remain unchanged (they are not shown in the figures). However, the white light irradiation using a mercury lamp through a water filter leads to an increase in the paramagnetic part of the $\mu_{eff}(T)$ curve, whereas the low-temperature part characterizing the ferromagnetic state remains unchanged (see Fig. 12). In compound **2**, analogous photoinduced changes in the high-temperature region are observed under UV light. This result is in good agreement with the data on the ferromagnetic effect in spiropyran iodides,[24] for which analogous photoinduced changes were observed in the high-temperature part of the plot $M(T)$. In spiropyran iodides, the photomagnetic effect is attributed to the generation of high-spin paramagnetic centers under irradiation. These data suggest that the photomagnetic effect in compound **3** has the same nature as that in spiropyran iodides of the indoline series, *i.e.*, the increase in the magnetic moment is attributed to radiation defects, which are accumulated after the photoexposure regardless of whether the open or closed form of the molecules is present in the crystals.

Therefore, the investigation of the molecular and crystal structure of salt **1**, which is used as the starting compound in the synthesis of mono- and bimetallic complexes **2** and **3**, showed that the C_{Sp}—O bond length in the chromenium cation of **1** is similar to that in photochromic salts of spiropyrans of the indoline series, but the observed crystal packing does not facilitate the isomerization of molecule **1** in the solid state. In compound **1**, no efficient photochromic transformations occur, which is apparently also associated with the absence of orbital n—σ* interactions in the chromenium cations.

Compound **1** is paramagnetic with the low-lying thermally excited states of the chromene molecules. At low temperatures (~2 K), the paramagnetic state is frozen, and compound **1** exhibits diamagnetic properties.

Compound **2** is paramagnetic, Cr^{3+} ions contribute to the magnetic properties, and the additional magnetic moment associated with the thermally induced paramagnetism of chromene molecules is observed at temperatures above 2 K.

At high temperatures (3—300 K), the magnetic moment of compound **3** in the paramagnetic region consists of the contributions of the paramagnetic Cr^{3+} and Mn^{2+} ions and the contribution of the light-sensitive thermally induced paramagnetic states of chromenes. At low temperatures (2—3 K), the thermally induced magnetism of organic molecules is frozen, and the ferro- or ferrimagnetic ordering (and, presumably, the spin-glass state) is observed in the two-dimensional sublattice of metal oxalates. The magnetic state of compound **3** is insensitive to the exposure of samples under white or UV light at low temperatures.

Based on the above-considered results, possible ways can be proposed to improve the methods for the synthesis of photochromic magnets. To efficiently control the magnetic subsystem of metal spins, it is necessary that the thermally induced spins of a photochromic subsystem be not frozen at magnetic ordering temperatures. This can be achieved either by increasing T_c for the anion subsystem or by decreasing the activation energy of the triplet states in the cation subsystem. The intersection of the temperature regions of the existence of the ferromagnetic ordering and the thermally induced triplet states can lead to the inclusion of the spins of photochromic molecules into ferromagnetic or antiferromagnetic interactions. In this case, it would be expected that the photoinduced transformations of the structures of photochromic molecules would efficiently influence the magnetic ordering.

We thank E. A. Yur´eva and A. N. Nekrasov for assistance.

This study was financially supported by the Presidium of the Russian Academy of Sciences (Program No. 18 "Development of Methods for the Synthesis of Chemical Compounds and the Design of New Materials," Project

"Fundamental Principles of the Design and Investigation of New Compounds and Materials for Molecular Electronics and Spintronics").

References

1. *Organic Photochromic and Thermochromic Compounds*, Eds J. C. Crano, R. J. Guglielmetti, Plenum, New York, 1999, Vol. **2**, 484.
2. V. I. Minkin, *Chem. Rev.*, 2004, **104**, 2751.
3. M. M. Krayushkin, *Khim. Geterotsikl. Soedin.*, 2001, 19 [*Chem. Heterocycl. Compd.* (*Engl. Transl.*), 2001, **37**].
4. V. Lokshin, A. Sama, A. V. Metelitsa, *Usp. Khim.*, 2002, **71**, 1015 [*Russ. Chem. Rev.* (*Engl. Transl.*), 2002, **71**].
5. S. Benard, P. Yu, *Adv. Mater.*, 2000, **12**, 48.
6. S. Benard, P. Yu, *J. Chem. Soc., Chem. Commun.*, 2000, 65.
7. S. M. Aldoshin, L. A. Nikonova, V. A. Smirnov, G. V. Shilov, N. K. Nagaeva, *Izv. Akad. Nauk, Ser. Khim.*, 2005, 2050 [*Russ. Chem. Bull., Int. Ed.*, 2005, **54**, 2113].
8. S. M. Aldoshin, L. A. Nikonova, V. A. Smirnov, G. V. Shilov, N. K. Nagaeva, *J. Mol. Struct.*, 2005, **750**, 158.
9. S. M. Aldoshin, L. A. Nikonova, G. V. Shilov, E. A. Bikanina, N. K. Artemova, V. A. Smirnov, *J. Mol. Struct.*, 2006, **794**, 103.
10. N. A. Sanina, S. M. Aldoshin, G. V. Shilov, E. V. Kurganova, E. A. Yur´eva, N. A. Voloshin, V. I. Minkin, V. A. Nadtochenko, R. B. Morgunov, *Izv. Akad. Nauk, Ser. Khim.*, 2008, 1424 [*Russ. Chem. Bull., Int. Ed.*, 2008, **57**, 1451].
11. S. Benard, E. Riviere, P. Yu, K. Nakatani, J. F. Delonis, *Chem. Mater.*, 2001, **13**, 159.
12. I. Kashima, M. Okubo, Y. Ono, M. Itoi, N. Kida, M. Hikita, M. Enomoto, N. Kojima, *Synth. Met.*, 2005, **155**, 703.
13. S. M. Aldoshin, N. A. Sanina, V. I. Minkin, N. A. Voloshin, V. N. Ikorskii, V. I. Ovcharenko, V. A. Smirnov, N. K. Nagaeva, *J. Mol. Struct.*, 2007, **826**, 69.
14. S. M. Aldoshin, N. A. Sanina, V. A. Nadtochenko, E. A. Yur´eva, V. I. Minkin, N. A. Voloshin, V. N. Ikorskii, V. I. Ovcharenko, *Izv. Akad. Nauk, Ser. Khim.*, 2007, 1055 [*Russ. Chem. Bull., Int. Ed.*, 2007, **56**, 1095].
15. S. M. Aldoshin, *Izv. Akad. Nauk, Ser. Khim.*, 2008, 704 [*Russ. Chem. Bull., Int. Ed.*, 2008, **57**, 718].
16. J. Berthet, S. Delbaere, D. Levi, A. Samat, R. Guglielmetti, G. Vermeersch, *Photochem. Photobiol. Sci.*, 2002, **1**, 665.
17. J.-L. Pozzo, A. Samat, R. Guglielmetti, R. Dubest, J. Aubard, *Helv. Chim. Acta*, 1997, **80**, 725.
18. G. M. Sheldrick, *SHELXTL v. 6.14*, *Structure Determination Software Suite*, Bruker AXS, Madison, Wisconsin, USA, 2000.
19. V. V. Tkachev, S. M. Aldoshin, N. A. Sanina, B. S. Luk´yanov, V. I. Minkin, A. N. Utenyshev, K. N. Khalanskii, Yu. S. Alekseenko, *Khim. Geterotsikl. Soedin.*, 2007, 690 [*Chem. Heterocycl. Compd.* (*Engl. Transl.*), 2007, **43**].
20. *GAUSSIAN 03. Rev. D01*, Gaussian, Inc., 340 Quinnipiac Street, Building 40, Wallingford, CT 06492.
21. G. V. Shilov, L. O. Atovmyan, N. S. Ovanesyan, N. A. Sanina, *Koord. Khim.*, 2001, **27**, 46 [*Russ. J. Coord. Chem.* (*Engl. Transl.*), 2001, **27**].
22. G. V. Shilov, N. S. Ovanesyan, N. A. Sanina, L. O. Atovmyan, M. Gruselle, *Koord. Khim.,* 2001, **27**, 605 [*Russ. J. Coord. Chem.* (*Engl. Transl.*), 2001, **27**].
23. M. Mitsumi, M. Ohba, M. Kodera, N. Matsumoto, *Bull. Chem. Soc. Jpn*, 1994, **67**, 2139.
24. R. B. Morgunov, F. B. Mushenok, S. M. Aldoshin, N. A. Sanina, G. V. Shilov, E. A. Yurieva, V. V. Tkachev, *New J. Chem.*, 2009, **33**, 1374.
25. A. Carrington, A. D. McLachlan, *Introduction to Magnetic Resonance with Application to Chemistry and Chemical Physics*, HARPER and ROW, New York—Evaston—London, 1967, 447 pp.
26. G. A. Vinogradov, I. A. Misurkin, A. A. Ovchinnikov, *Theor. Exp. Chem.*, 1973, **12**, 723.
27. Y. Morita, T. Aoki, K. Fukui, S. Nakazawa, K. Tamaki, S. Suzuki, A. Fuyuhiro, K. Yamamoto, K. Sato, D. Shiomi, A. Naito, T. Takui, K. Nakasuji. *Angew. Chem., Int. Ed.*, 2002, **41**, 1793.
28. S. Nelsen, R. Ismagilov, Y. Teki, *J. Am. Chem. Soc.*, 1998, **120**, 2200.
29. L. Xu, T. Sugiyama, H. Huang, Z. Song, J. Meng, T. Matsuura, *Chem. Commun.*, 2002, **20**, 2328.
30. K. Matsuda, M. Irie, *Chem. Lett.*, 2000, 16.
31. A. Minsky, A. Y. Meyer, R. Poupko, M. Rabinovitz, *J. Am. Chem. Soc.*, 1983, **105**, 2164.
32. B. L. Nordo, Z. G. Soos, H. M. McConnell, *Ann. Rev. Phys. Chem.*, 1966, **17**, 237.
33. T. S. Cameron, A. Decken, R. M. Kowalczyk, E. J. L. McInnes, J. Passmore, J. M. Rawson, K. V. Shuvaev, L. K. Thompson, *Chem. Commun.*, 2006, 2277.

Received June 18, 2009;
in revised form November 12, 2009